Tight-binding molecular-dynamics simulations of amorphous silicon carbides

V. I. Ivashchenko,[1] P. E. A. Turchi,[2] V. I. Shevchenko,[1] L. A. Ivashchenko,[1] and G. V. Rusakov[1]
[1]*Institute of Problems of Materials Science, NAS of Ukraine, Krzhyzhanovsky Street 3, 03142 Kyiv, Ukraine*
[2]*Lawrence Livermore National Laboratory, L-353, P.O. Box 808, Livermore, California 94551*
(Received 18 May 2002; published 6 November 2002)

Atomic and electronic structures of amorphous tetrahedral silicon carbide *a*-SiC are analyzed on the basis of molecular dynamics simulations performed in the framework of a sp^3s^* tight-binding force model. The *a*-SiC samples are generated from dilute vapors and melts. The topology and the local chemical order of the resulting amorphous networks are very sensitive to the initial high-temperature structures. The simulations are used to investigate the electronic distribution in the band gap region and the changes in the density of states caused by the presence of homo-polar bonds, coordination defects, and strongly distorted tetrahedral species. For completeness the results obtained for *a*-SiC are compared with those from various semiempirical schemes and from *ab initio* pseudopotential calculations.

DOI: 10.1103/PhysRevB.66.195201 PACS number(s): 61.43.Dq, 71.15.Pd, 71.23.Cq

I. INTRODUCTION

In contrast to amorphous silicon and carbon that were extensively studied by different methods,[1–4] theoretical works devoted to the investigation of amorphous silicon carbide (*a*-SiC) are rather sparse. Previous studies on condensed *a*-SiC are based on two different approaches, namely, *ab initio* molecular dynamics (MD) simulations within the pseudopotential approach (PA) (Refs. 5–7) and Monte Carlo (MC) simulations based on the empirical potential (EP) of Tersoff.[8–10] The density of states (DOS) was computed for small size systems using the PA within the local density approximation (LDA) for exchange-correlation potential that describes the electron-electron interaction. The resulting DOS does not show a distinct semiconducting band gap (BG), though the DOS of a 54-atom sample[5] has a distinct pseudogap that suggests the tendency towards gap formation. Although both methods allow an accurate determination of the atomic distribution in *a*-SiC the electronic DOS determined from the *ab initio* approach is computed incorrectly, since the LDA is known to underestimate BG.[6] For comparison, the width of the BG (Eg) for the diamondlike structure of SiC (3C-SiC, also named β-SiC) ranges from 1.24 to 1.27 eV according to PA calculations,[11–13] much smaller than the experimental value of 2.39 eV.[14] The authors of Ref. 15 have introduced an additional contribution to the exchange-correlation potential in an *ad hoc* way to obtain a band gap of 2.52 eV with the linear muffin-tin orbital (LMTO) method. We have shown in previous studies[16,17] that the gap problem could be partially overcome by carrying out band structure calculations for the atomic structure of *a*-SiC generated by EP-MD simulations. However, regardless of the efficiency of the sp^3s^* tight-binding (TB) method used in investigating the final DOS, this approach lacked consistency since the electronic subsystem was not involved in the MD simulations. Therefore, in this paper we consider both the atomic and electronic subsystems of *a*-SiC by using a procedure capable of providing the appropriate atomic distribution and of describing the electronic states in the BG region within the same electronic structure approach. The sp^3s^* TB orthogonal interpolation scheme[18] was used to calculate the DOS during the MD simulations. Here, we have to stress that a sp^3 scheme is not able to describe the indirect band gap correctly [associated with the transitions from Γ'_{25} to Δ_1 and from Γ_{25} to X_1 (Ref. 18) in *c*-Si and in 3C-SiC]. However, the introduction of the additional s* state in the sp^3s^* TB scheme makes it possible to reproduce the BG in accordance with experiment. In addition, in contrast to the PA-MD scheme that depends on plane-wave expansion of the electronicwave functions,[1,4–7] the TB calculations only require a few atomic orbitals centered on each atom, and therefore this latter approach is suitable for carrying out simulations for large size samples and over a long time. In addition, in the TB-MD approach, the electronic degrees of freedom do not enter explicitly in the MD simulations, and therefore the problem of heating the electronic subsystem encountered in the PA-MD scheme is avoided. The additional parameters of the repulsion contribution to the energy in the TB scheme were determined from pseudopotential calculations. The atomic distribution and the influence of threefold coordinated (T_3), fivefold coordinated (T_5), and strongly distorted fourfold coordinated (T_4) atoms on the electronic structure of *a*-SiC were studied in the framework of sp^3s^* TB-MD approach. Several MD calculations were carried out under different conditions to validate the possibilities afforded by this approach. The sp^3s^* TB-MD results are compared with those of other authors when available. The paper is organized as follows. In Sec. II, the details of the computational scheme are presented. In Sec. III, we report the results that pertain to both the structural and the electronic properties of *a*-SiC with comparison to previously published data. Finally, results are briefly summarized in Sec. IV.

II. COMPUTATIONAL ASPECTS

In this work, MD simulations based on the sp^3s^* tight-binding orthogonal interpolation scheme[18] was employed to reproduce with great accuracy both the atomic distribution and the electronic structure of *a*-SiC. In our variant of the TB-MD scheme, a pairwise potential that accounts for the ion-ion repulsive interactions and the correction to the double counting of the electron-electron interactions is con-

TABLE I. Tight-binding parameters (eV), cutoff distances R_0 (Å), bond length r_0 (Å), and potential parameters, see Eq. (1), U_1, U_2 (eV) and r_D (Å) used in the present work.

	Si		SiC		C
		Si		C	
E_s	-4.322	-3.641		-8.441	-8.441
E_p	1.328	3.359		0.959	0.459
E_s^*	13.583	14.059		15.059	14.997
R_0	2.5-2.9	2.2		2.2	1.9
$ss\sigma$	-1.897		-2.714		-3.758
$sp\sigma$	-2.125	-3.429		-3.340	-4.898
$pp\sigma$	2.632		4.623		5.809
$pp\pi$	-0.818		-1.135		-1.775
$ss^*\sigma$	-0.122	0.000		0.000	0.511
$s^*p\sigma$	-2.970	2.779		4.646	-3.063
r_0	2.340	1.890		1.890	1.564
U_1	2.4513		4.6549		7.0048
U_2	0.9670		1.2159		2.3243
r_D	0.3156		0.3038		0.2937

sidered, and takes the following form:[19]

$$V(r) = U_1 \exp\left(- \frac{r - r_0}{r_D} \right) + U_2 \frac{r_0}{r}, \tag{1}$$

where r is the distance between neighboring atoms, r_0 is its equlibrium counterpart in the ZnS phase, and U_1, U_2, and r_D are the parameters defined for Si-Si, Si-C, and C-C pairs.

The potential parameters introduced in Eq. (1) are determined from total energy calculations carried out for *c*-Si, *c*-C, and 3C-SiC in the rock-salt and diamondlike structures using a first-principles PA method. The *ab initio* calculations are based on norm-conserving pseudopotentials constructed according to the scheme of Hamann,[20] and represented in the fully separable form.[21] The Brillouin zone (BZ) integration over the *k* points is replaced by a discrete sum over a set of 10 special *k* points according to the Monkhorst-Pack scheme.[22] The cutoff energy for the Kohn-Sham plane-wave basis set is taken at 35 Ry, and the exchange-correlation energy is expressed within the local density approximation.[23,24] The parameters of the sp^3s^*-TB scheme for 3C-SiC, *c*-Si, and *c*-C were carefully determined and discussed in an earlier study.[16,17] Therefore, here we only note that our scheme gives BG of 1.17, 2.40, and 5.50 eV for *c*-Si, 3C-SiC, and *c*-C, respectively, which are close to their experimental counterparts. The distance-dependence of the two-center hopping parameters was chosen according to the Harrison rule.[25] The parameters of the sp^3s^*-TB scheme and of the pairwise repulsive potential given in Eq. (1) are presented in Table I.

The MD simulations were carried out at constant volume (for the exception of the simulation of a dilute vapor phase, where a cell volume was varied), and the equations of motion were solved with a standard velocity-Verlet algorithm.[26] Periodic boundary conditions were applied to a stoichiometric supercell of 54, 64, 128, or 216 atoms with an atomic density that was equal to the one of the 3C-SiC crystalline compound. Simulations were performed for a cubic cell by quenching from the melt or by homogeneously condensing the vapor (the latter starting state will be referred to as *V* in the following). In the first procedure, to generate a liquid configuration of SiC, the diamondlike (*D*) or rock-salt (*B*) structures were heated for 2 ps at 4000 K. Along with TB-MD we have performed MD simulations based on the empirical potential of Tersoff with a carbon potential defined from graphite (EP-64 K sample)[27] and from diamond (EP-64T sample),[28] in which case the melts were prepared at 8000 K from the diamondlike structure.[10] In the second procedure, our starting state is the dilute vapor phase. The initial cubic cell has a lattice parameter that is 1.5 times larger than the one of the 3C-SiC crystal and contains randomly distributed atoms far apart from each other. The cells are allowed to slowly shrink under applied pressure at 2000 K during about 2 ps. To reach full equilibrium the high-temperature structures were slowly quenched with an average cooling rate of $1-5\times10^{14}$ K/s down to 300 K. The EP-based samples were cooled more slowly with $r_{\mathrm{cool}}\sim10^{-13}$ s, using a time step h of 0.8×10^{-16} s. In the TB-MD simulations we have considered different h values depending on sample sizes. For the 54- and 64-atom samples, $h\sim5\times10^{-15}$ s, whereas for the 129 and 216 atom samples, $h\sim10^{-14}$ s. Despite the use of comparable large time steps the MD process was stable, i.e., the potential energy variations did not exceed 5–10 meV/atom. The *a*-SiC samples generated according to these two procedures were then averaged for about 2 ps to achieve thermal equilibrium. The thermal equilibration was carried out without any further relaxation.

The DOS of *a*-SiC required for TB-MD simulations was computed at the center of the BZ, and the final DOS was constructed by using the eigenvalues at 165 and 35 *k* points of the irreducible wedge of the BZ when simulating the small- and large-size samples, respectively. An analysis of the local DOS was carried out in the framework of the recursion technique first introduced by Haydock, Heine, and Kelly,[29] and Nex.[30] The initial MD-cell was duplicated according to the periodic boundary conditions selected during the simulations to generate a large cluster of 4096 atoms. The local DOS of various *a*-SiC systems were obtained using the recursion coefficients of 54 levels of continued fraction that describe the single-electron Green function. The partial DOS $n_{n\lambda}(E)$ per site n and per orbital λ is related to the single-electron Green function $G_{n\lambda}(z)$ by

$$n_{n\lambda}(E) = -\frac{1}{\pi} \mathrm{Im} \lim_{\eta \to 0^+} G_{n\lambda}(E + i\eta), \tag{2}$$

with the following continued fraction expansion for the partial Green function:

$$G_{n\lambda}(z) = \cfrac{b_{1,n\lambda}^2}{z - a_{1,n\lambda} - \cfrac{b_{2,n\lambda}^2}{z - a_{2,n\lambda} - \cfrac{b_{3,n\lambda}^2}{z - \cdots}}}, \tag{3}$$

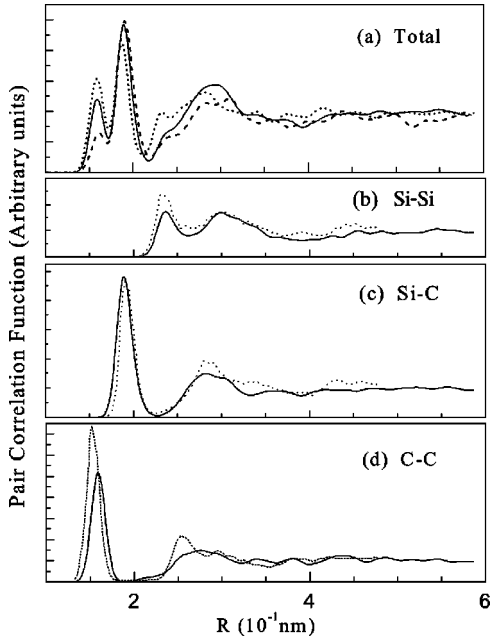

FIG. 1. Total (a) and partial (b)–(d) pair correlation functions (PCF) of *a*-SiC. (a) TB-216B (solid line), TB-64B (dashed line), and TB-128V1 (dotted line); (b)–(d) TB-216B (solid line) and PA-54 (dotted line).

and the coefficients of the continued fraction $\{a_{p,n\lambda}, b^2_{p,n\lambda}\}$ are calculated according to the Lanczos algorithm that constitutes the basis of the recursion technique. In the present study, the maximum number (54) of coefficients was selected to guarantee the convergence of the DOS for the periodic SiC compound.

III. RESULTS AND DISCUSSION

A. Structural properties

In Fig. 1, we show the total and partial pair-correlation functions (PCF's) of *a*-SiC samples prepared from different precursors and under various conditions of MD simulations. The characteristics of the samples are given in Table II. From these results one can single out one characteristic feature: all the PCF curves are similar. They only differ in the relative magnitude of the peaks associated with the distribution of nearest neighbor Si-Si, Si-C, and C-C pairs. The main peak positions are centered around the mean values of 0.235 ± 0.003 nm, 0.189 ± 0.004 nm, and 0.156 ± 0.002 nm, associated with the Si-Si, Si-C, and C-C pairs, respectively. By inspection of Fig. 1 and Table II, we deduce that the final amorphous structure depends on the precursor and, to a lesser extent, on sample size. It is clearly seen that the cooling of the melts leads to more chemically ordered structures (the structure with the maximal number of Si-C bonds) than the quenching of dilute vapors.

Given the number of homopolar bonds in our samples, we deduce that the 128 atom samples are chemically disordered, as was found for the 54 atom sample by Finocchi *et al.*[5] Other samples demonstrate moderate chemical order, which close to the findings of the authors.[6–9] An imperfection in the amorphous network, which is characterized by the extent of a deviation from the ideal tetrahedral coordination, is less sensitive to the precursor and to the cluster size. However, the alloys obtained at the slower cooling rates are more perfect compared with the rapidly quenched samples. The situation is partially clarified by inspection of the PCF of two high-temperature structures from which the amorphous

TABLE II. Structural parameters of *a*-SiC samples obtained by different authors. R_{Si} is the cut-off distance of the Si-Si interactions (since the Si-Si PCF has not the distinct dip restricting the nearest neighbor correlations, in our calculations this distance was chosen to maximize the number n_4). In our calculations $R_{\mathrm{C\text{-}C}}$ and $R_{\mathrm{Si\text{-}C}}$ were equal to 0.19 and 0.22 nm, respectively; n_i is the percentage of i-fold coordinated atoms; N_i is the average coordination number of species i; N_{i-j} is the percentage of i-j bonds in the sample. Abbreviation in the sample notation should read as follows: method number of atoms in a cluster-high-temperature precursor (*B*: rock salt, *D*: diamondlike, *V*: dilute vapor). The *V*2 sample was cooled two times slower than the *V*1 sample.

Sample	R_{Si} (nm)	n_3 (%)	n_4 (%)	n_5 (%)	n_6 (%)	N_{Si}	N_{C}	$N_{\mathrm{Si\text{-}Si}}$ (%)	$N_{\mathrm{Si\text{-}C}}$ (%)	$N_{\mathrm{C\text{-}C}}$ (%)
TB-54*V*	0.252	9.3	83.3	5.5	1.9	4.04	3.96	18.5	63.8	17.7
TB-64*V*	0.246	12.5	79.7	6.3	1.5	4.00	3.94	20.5	59.8	19.7
TB-64*B*	0.255	12.5	75.0	12.5	0.0	4.03	4.00	12.5	75.8	11.7
TB-128*V*1	0.247	11.7	82.0	6.3	0.0	3.94	3.95	25.4	49.2	25.4
TB-128*V*2	0.248	6.3	84.4	9.3	0.0	4.09	3.97	24.0	53.5	22.5
TB-216*D*	0.260	9.3	86.1	4.6	0.0	3.96	3.94	2.8	94.6	2.6
TB-216*B*	0.254	5.6	85.2	8.8	0.4	4.10	3.98	20.9	60.3	18.8
EP-64*K*	0.260	48.4	46.9	4.7	0.0	3.94	3.19	29.8	50.9	19.3
EP-64*T*	0.255	7.8	76.6	15.6	0.0	4.22	3.94	20.7	62.4	16.9
PA-54 [a]	0.250	17	77	6	0	3.93	3.85	23	53	24
PA-16 [b]	N/A	0	100	0	0	4.00	4.00	7–16	68–84	7–16

[a]Reference 5.
[b]Reference 6.

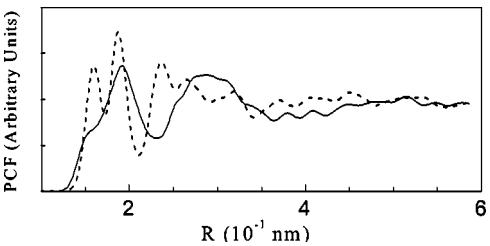

FIG. 2. Pair correlation function (PCF) of the condensed dilute vapor at 2000 K (dashed line) and of the melt of SiC in the rock-salt structure at 4000 K (solid line).

samples were obtained. The atomic distributions in the melt prepared by melting SiC in the rock-salt structure and by condensing a dilute SiC vapor at 2000 K are shown in Fig. 2. One can see that, in the liquid, in contrast to the condensed high-temperature structure, the Si-C correlations show up more clearly. Hence, the amorphous nature of the resulting network generated from the melt will be better achieved.

For comparison, we also present in Figs. 1(b)–1(d) the local PCF of the PA-54 sample generated using the first-principle pseudopotential approach.[5] It is seen that the atomic distribution of the TB-216B sample, which is typical for all our samples, is very similar to that of the PA-54 alloy. However, noticeable differences exist in the region of the second nearest neighbor interactions. In our samples this region is more diffuse than in the PA-54 sample. In addition, the main peak of C-C correlations for our sample is shifted toward larger distances compared to the analogous peak for the PA-54 sample, and this can be attributed to the larger equilibrium lattice parameter for diamond used in our approach (0.1564 nm compared with the value of 0.1540 nm obtained experimentally). Table II also shows some characteristics of the amorphous samples obtained by other authors. Based on these results we note that our samples differ from the PA-54 alloy by a smaller content of T_3 atoms and from the EP-64*T* by a more homogeneous distribution of Si atoms. Otherwise, all the samples have very similar atomic-structure characteristics except for the EP-64*K* sample that will be considered below.

In Fig. 3 the bond-angle distributions $g(\theta)$ for four amorphous alloys are displayed. The tetrahedral character of the amorphous network is confirmed by the function $g(\theta)$ in the two upper panel. Figure 3(a) demonstrates that regardless of almost the same number of coordination defects in the TB-216D and TB-216B samples their band-angle distributions differs, mostly due to the difference in the number of homopolar bonds (Table II). The latter promotes the increase of strongly distorted sites which leads to broadening $g(\theta)$. In Fig. 3(b) the main structure is located around 107.8°. The shoulder around 120°–130° can be attributed to T_3 silicon and carbon atoms. The distribution for Si is broader than the one for C, and this indicates that the Si atoms are distributed more randomly than the C atoms. The function $g(\theta)$ of the EP-64*K* sample exhibits the graphitelike character of the *a*-SiC network with the main peak around 120°. For this sample, both the silicon and carbon atoms exhibit mostly the sp^2 bonding character. Apparently, the latter observation is explained by the specificity of the empirical potential for

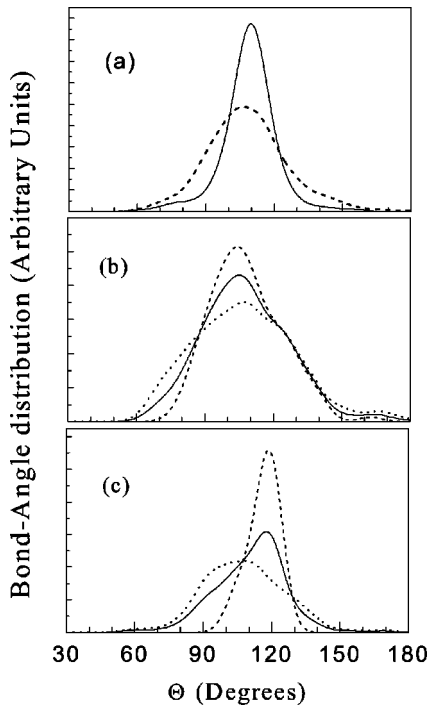

FIG. 3. Bond-angle distributions $g(\theta)$ in the TB-216*D* (solid line) and TB-216*B* (dashed line) samples (a), $g(\theta)$ of Si (dotted line), C (dashed line), and Si+C (solid line) in *a*-SiC obtained by using TB-MD [TB-128*V*1 sample (b)] and the EP-MD [EP-64 K sample (c)].

carbon, which was determined from the data pertaining to graphite.[27] We note that the characteristics of the EP-64*K* sample presented in Table II are very close to those of the 216-atom sample generated by the MC simulations.[9] However, the latter sample is more perfect than EP-64*K* because of the use of different computational schemes. MC simulations usually generate less defective structures than MD simulations,[9,10] although one would anticipate that MD simulations closely mimic the experimental procedures that are used to prepare amorphous materials.

B. Electronic structure properties

The total densities of states associated with various samples are shown in Fig. 4. By simple inspection of the distributions of electronic states in *a*-SiC alloys it is easy to show that the DOS in the ionicity gap (IG) region (at about -11 eV) and the semiconducting gap (BG) region (in the range -1.2 to +1.2 eV) is very sensitive to the structural properties of the amorphous network. First of all, it is clearly seen that both the IG and BG contain deep levels associated with coordination defects and with distortions in the tetrahedrally coordinated sites. The DOS of the chemically random and relaxed 3C-SiC crystal points out that the presence of homo-polar bonds modifies the spectrum in the IG region and leads to a smearing of the fine structure of the valence and conduction bands. The IG is absent in the chemically disordered SiC crystal (with about 50% of homopolar bonds). Thus, the peaks at −14 and −10 eV, and the low densities of states at −11 and −7 eV become more distinct

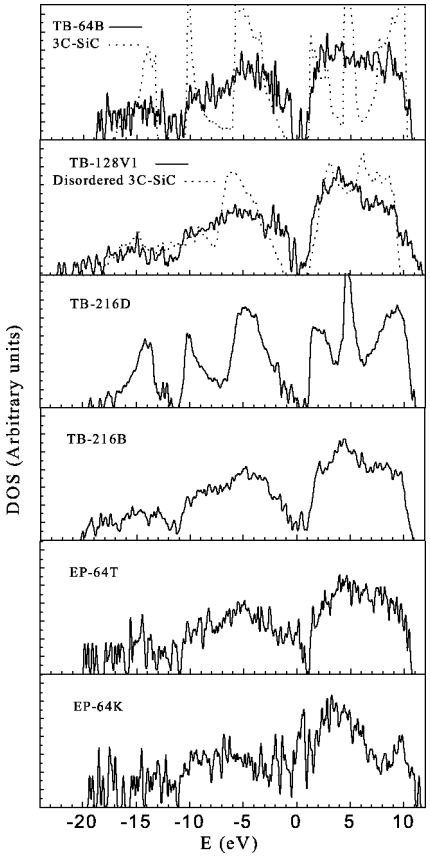

FIG. 4. Eigenvalues-based total density of states (DOS) of several simulated *a*-SiC. The Fermi energy corresponds to the zero of energy.

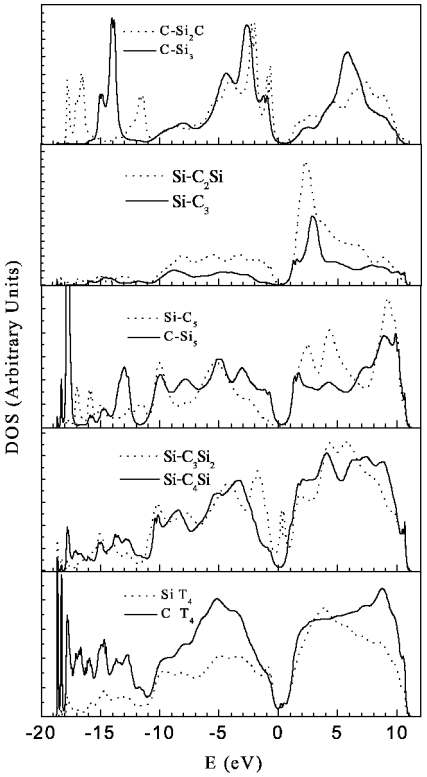

FIG. 5. Local densities of states (DOS) of silicon and carbon atoms located in different local environments, as obtained by the recursion technique. The Fermi energy corresponds to the zero of energy.

with a decrease in the number of homopolar bonds. Correspondingly, these features in the electronic spectrum of *a*-SiC can be considered as the indicator of chemical order. Homopolar bonds widen the dip in the BG region whereas, at the same time, the bandgap width remains unchanged. This result is consistent with the data obtained for single antisite defects in 3C-SiC by the LMTO method.[31] Taking into account these findings and the DOS of the *a*-SiC samples with various degrees of chemical order, we conclude that the scattering in the BG width is mostly caused by coordination defects and by the magnitude of the deformation in the tetrahedral configurations. On the other hand, it is the extent of topological order that determines the shape of the DOS inside the BG. Here we note that this conclusion contradicts the findings of Ref. 6. Indeed, in this study the authors concluded that a strengthening of the dip in the BG region was associated with an increase in chemical order, whereas we attribute this same feature to an improvement in the amorphous network of the generated samples, since homopolar bonds promote a creation of strongly distorted sites [Fig. 3(a)].

As far as the influence of defects on the DOS is concerned, particularly in the BG region, we singled out the set of gap levels that are located in the valence band (VB) tail (around -1.2 eV), in the midgap region and in the conduction band (CB) tail (around +1.2 eV). To clarify the origin of these gap levels, we have calculated the local DOS related to the atoms positioned in different local environments. The electronic spectra computed by the recursion technique are shown in Fig. 5. Because of the finite number of computed levels of continued fraction the DOS has smooth band edges compared with the eigenvalue-based DOS.[32] In addition, although the application of the recursion technique can lead to spurious peaks in the DOS, especially at the band edges of the electronic spectrum and for small size samples, it provides the correct positions in energy of the resonance and gap levels in the local DOS.[29,30] The analysis of the local DOS makes it possible to single out the contribution to gap states from various atomic configurations. The dangling-bond states of T_3 carbon atoms contribute to the VB tail and to the midgap, in contrast to the analogous silicon states that form both in the VB and CB tails. The distribution of gap states related to the T_5 carbon atoms resembles that of T_3 carbon atoms, which is consistent with the model of defect states in *a*-Si by Pantelides.[33] Floating-bond states of the Si-C_5 and Si-C_4Si configurations are diffused in the band tails. A similar distribution of floating-bond states was detected in Ref. 34 for *a*-Si. The localized peak in the midgap region around 0.4 eV originates from T_5 silicon atoms in the C_3Si_2 surroundings. The gap states belonging to the T_4 silicon and carbon atoms are scattered all over the BG region. These findings show that the position of the gap states is determined not only by coordination defects but also by the distribution of homopolar bonds. This picture of the interatomic interactions in *a*-SiC confirms the conclusions of the appli-

cation of a band model that we considered in an earlier work.[16,17] However, the present findings are more reliable and consistent, since they are based on the results of MD simulations based on the same TB electronic model Hamiltonian. This is confirmed by the results of DOS obtained for a 64 atom sample. Although the TB-64*B* sample has a denser defect structure than the one of the EP-64*T* alloy, its DOS in the BG region has the distinct broad dip in contrast to the DOS of the EP-64*T* sample, in which the BG is shown as a narrow minimum around 1 eV in Fig. 4. In the TB-MD scheme, peculiarities of the electronic structure of the generated samples are taken into account in the process of MD simulations. In contrast, in EP-MD calculations, an amorphous network is formed according to a pair-potential scheme of interatomic interactions in which the electronic structure (and in particular the gap states) does not play any role.

IV. CONCLUSION

We have investigated the atomic and electronic structure properties of *a*-SiC using a sp^3s^* TB-MD scheme. The rather good agreement between the characteristics obtained with the present method and with *ab initio* MD validates to a great extent the efficiency and the accuracy of our approach. The amorphous samples studied in this work display various degrees of chemical order depending on the preparation conditions, however they all display 6 to 13 % of undercoordinated and overcoordinated sites. The *a*-SiC network generated from the dilute vapors differs from the one obtained from the melt because of a significantly reduced number of heteropolar bonds in the vapor. The existence of ionicity-gap states is mostly explained by the presence of homopolar bonds. The abnormally coordinated atoms and the strongly distorted tetrahedrally coordinated species give rise to additional states in the semiconducting gap region. Carbon and silicon dangling-bond states are localized at the bottom of the gap and at the band tails, respectively. Overcoordinated atoms give rise to both localized and diffuse gap states. Finally the presence of strongly distorted fourfold coordinated atoms gives rise to states in the entire energy window that characterizes the semiconducting band gap. This approach will then be used to predict properties of *a*-SiC that are observed under various experimental conditions in bulk samples as well as in thin films, and the results will be reported in a forthcoming publication.

ACKNOWLEDGMENTS

This work was supported in part by STCU Contract No. 1591. The work of P. T. was performed under the auspices of U. S. Department of Energy by the University of California Lawrence Livermore National Laboratory under Contract No. W-7405-ENG-48.

[1] I. Stich, R. Car, and M. Parrinello, Phys. Rev. B **44**, 11 092 (1991).
[2] E. Kim and Y. H. Lee, Phys. Rev. B **49**, 1743 (1994).
[3] M. Peressi, M. Fornari, S. D. Girodcolli, L. D. Santis, and A. Baldereschi, Philos. Mag. **80**, 515 (2000).
[4] G. Galli, R. M. Martin, R. Car, and M. Parrinello, Phys. Rev. B **42**, 7470 (1990).
[5] F. Finocchi, G. Galli, M. Parrinello, and C. M. Bertoni, Phys. Rev. Lett. **68**, 3044 (1992).
[6] P. C. Kelires and P. J. N. Denteneer, Solid State Commun. **87**, 851 (1993).
[7] P. C. Kelires and P. J. N. Denteneer, J. Non-Cryst. Solids **231**, 200 (1998).
[8] P. C. Kelires, Europhys. Lett. **14**, 43 (1991).
[9] P. C. Kelires, Phys. Rev. B **46**, 10 048 (1992).
[10] J. Tersoff, Phys. Rev. B **49**, 16 349 (1994).
[11] C. H. Park, B.-H. Cheong, K.-H. Lee, and K. J. Chang, Phys. Rev. B **49**, 4485 (1994).
[12] P. Kackell, B. Wenzien, and F. Bechstedt, Phys. Rev. B **50**, 10 761 (1994).
[13] Including the results of pseudopotential based calculations performed in the present work.
[14] *Landolt Bornstein Tables*, edited by O. Madelung, M. Schulz, and B. Segall (Springer-Verlag, Berlin, 1984), Vol. 17.
[15] G. Gubiotti, Y. N. Kucherenko, and V. N. Antonov, J. Phys.: Condens. Matter **9**, 165 (1997).
[16] V. I. Ivashchenko and V. I. Shevchenko, Appl. Surf. Sci. **184**, 137 (2001).
[17] V. I. Ivashchenko, V. I. Shevchenko, G. V. Rusakov A. S. Klymenko, V. M. Popov, L. A. Ivashchenko, and E. I. Bogdanov, J. Phys.: Condens. Matter **14**, 1799 (2002).
[18] P. Vogl, H. J. Hjalmarson, and J. D. Dow, J. Phys. Chem. Solids **44**, 365 (1983).
[19] C. Molteni, L. Colombo and L. Miglio, Phys. Rev. B **50**, 4371 (1994).
[20] D. R. Hamann, Phys. Rev. B **40**, 2980 (1989).
[21] L. Kleinman and D. M. Bylander, Phys. Rev. Lett. **48**, 1425 (1982).
[22] H. J. Monkhorst and J. D. Pack, Phys. Rev. B **13**, 5188 (1976).
[23] D. M. Ceperley and B. J. Adler, Phys. Rev. Lett. **45**, 566 (1980).
[24] J. P. Perdew and A. Zunger, Phys. Rev. B **23**, 5048 (1981).
[25] W. A. Harrison, *Electronic Structure and Properties of Solids* (Freeman, San Francisco, 1980).
[26] L. Verlet, Phys. Rev. **159**, 98 (1967).
[27] J. Tersoff, Phys. Rev. B **39**, 5566 (1989).
[28] J. Tersoff, Phys. Rev. Lett. **64**, 1757 (1990).
[29] R. Haydock, V. Heine, and M. J. Kelly, J. Phys. C **5**, 2845 (1972).
[30] C. M. M. Nex, Comput. Phys. Commun. **43**, 101 (1984).
[31] G. Gubiotti, Y. Kucherenko, A. Yaresko, A. Perlov, and V. Antonov, J. Phys.: Condens. Matter **12**, 3369 (2000).
[32] P. Turchi, F. Ducastelle, and G. Treglia, J. Phys. C **15**, 2891 (1982).
[33] S. T. Pantelides, Phys. Rev. Lett. **57**, 2979 (1986).
[34] R. Biswas, C. Z. Wang, C. T. Chan, K. M. Ho, and C. M. Soukoulis, Phys. Rev. Lett. **63**, 1491 (1989).